Engineered Science

RESEARCH PAPER

View Article Online

Corrole functionalized iron oxide nanocomposites as enhanced peroxidase mimic and their application in H_2O_2 and glucose colorimetric sensing

Linna Gao,†[1] Leyou Zhang,†[1] Xintian Lyu,[3] Guifen Lu*[2] and Qingyun Liu*[1]

For the first time, functional Corrole molecules modified iron oxide (Fe_3O_4) magnetic nanoparticles (MNPs) were prepared by a facile two-step method. The Corrole-Fe_3O_4 nanocomposites exhibited a higher peroxidase-like activity than that of pure Fe_3O_4 nanoparticles, and accelerated the oxidation of peroxidase substrate 3,3',5,5'-tetramethylbenzidine (TMB) with the help of hydrogen peroxide (H_2O_2) only in 5 min, attributing to hydroxyl radicals (·OH) generated in the process of oxidation of TMB. Kinetic analysis showed that the catalytic behaviors followed the typical Michaelis-Menten kinetics. Additionally, Corrole-Fe_3O_4 exhibits several advantages including low cost, easy separation, facile fabrication, and high catalytic efficiency. Based on the catalytic activity of Corrole-Fe_3O_4 nanocomposites, a simple, sensitive, and selective colorimetric biosensor for H_2O_2 and glucose determination was successfully designed. The linear relationships of absorbance of oxidized TMB at 652 nm with H_2O_2 or glucose concentration were obtained from 10 μM to 100 μM with a detection limit of 3.6 μM and 4 μM to 40 μM with the detection limit as low as 2.46 μM, respectively. The results demonstrate that the Corrole-Fe_3O_4 nanocomposites have potential applications in bioanalysis and biodetection.

Keywords: Corrole; Corrole-Fe_3O_4; nanocomposites; peroxidase mimetic; colorimetric; glucose

Received 23rd February 2018, Accepted 6th March 2018

DOI: 10.30919/espub.es.180314

1. Introduction

Colorimetric biosensing associated with enzymes has gained considerable attention not only due to its simplicity and practicability but also without requirement for any expensive and sophisticated instruments.[1–9] It is known to us that the natural enzyme, HRP, has been playing key roles in colorimetric biosensing in the past few years. However, several limitations including expensive preparation and purification, low stability, and harsh storage, inhibited the application of natural enzyme,[10] thus leading to a high desire to construct and fabricate enzyme mimics with similar or even superior properties.[11,12]

Recently, with the development of study of nanomaterials,[13,14] more and more ferromagnetic nanoparticles have attracted considerable attention because of their large specific surface area and high surface reactivity[15–17] as well as their unique magnetic properties and potential applications in the fields of drug delivery,[18] biological separation[19] and biological catalysis.[20–23] For example, Fe_3O_4 magnetic nanoparticles (MNPs) generally considered to be biologically and chemically inert have been first reported to exhibit an intrinsic peroxidas-like catalytic activity,[24] which captures intense interesting in magnetic nanomaterial-related enzyme mimics. Subsequently, investigations about magnetic nanomaterial as alternatives to natural enzymes are further explored ranging from single magnetic nanoparticles to composites together with various potential applications in biocatalytic field. For example, Wang et al developed a coprecipitation method to prepare Fe_3O_4 MNPs and achieved the detection of H_2O_2 and glucose.[10–12] Chen et al established a colorimetric assay method for the detection of melamine using Fe_3O_4 MNPs.[25] Yan et al developed a novel Fe_3O_4 magnetic nanoparticle peroxidase mimetic based colorimetric method for the rapid detection of organophosphorus pesticides and nerve agents.[26] Furthermore, based on the Fe_3O_4 magnetic materials, various composited magnetic nanomaterials have been focused on.[27,28] Yuan et al investigated the enzyme-mimic activities of the Ag@Fe_3O_4 nanocomposite.[29] Kang et al reported a facile route to synthesize size tunable Fe_3O_4-carbon nitride nanotube (CNNT) hybrids with high peroxidase mimetic activity.[30] Gu et al found that Prussian blue modified iron oxide magnetic nanoparticles exhibited enhanced peroxidase-like catalytic activity.[31] Liu and coworkers have studied functional organic molecules modified magnetic nanoparticles which demonstrated the enhanced peroxidase mimetic activity.[32–34] The previous studies prove that people have paid attention to the nanocomposites based on magnetic materials as peroxidase mimics.

Corroles, which have a somewhat more condensed N4 coordination core and a much more electron-rich π system[35] have attracted enormous interest in recent years.[36–42] This is not only because of

[1] College of Chemical and Environmental Engineering, Shandong University of Science and Technology, Qingdao 266590, P. R. China. E-mail: qyliu@sdust.edu.cn
[2] School of Chemistry and Chemical Engineering, Jiangsu University, Zhenjiang 212013, P. R. China. E-mail: luguifen@ujs.edu.cn
[3] College of Liberal Arts, University of Minnesota, TwinCities, Minnesota, 55455, USA
† These authors contributed equally to this work

© Engineered Science Publisher LLC 2018

improved synthetic methods that make them more readily available but also because of their potential applications in the fields of photodynamic therapy, solar cells, catalysis and sensors.[39,40,43–45] Nowadays, its functionalization and further applications as catalysts, dyes for solar energy conversion and in medicine are attracting increasing interest.[39,43,46,47] However, up to date, there are no reports on using Corroles to modify Fe_3O_4 magnetic nanoparticles, which can be employed as colorimetric sensing materials to detect H_2O_2 and glucose.

In this work, for the first time, we selected functional Corrole molecules to modify iron oxide (Fe_3O_4) magnetic nanoparticles, which demonstrated the enhanced peroxidase-like activity. The Corrole functionalized Fe_3O_4 nanoparticles (Corrole-Fe_3O_4 nanocomposites) could accelerate to oxidize the peroxidase substrate 3,3',5,5'-tetramethylbenzidine (TMB) in the presence of H_2O_2, suggesting a higher catalytic activity than that of pure Fe_3O_4 nanoparticles. On the basis of the experimental results, we have successfully developed a simple, selective, colorimetric and visual method for detecting glucose (Scheme 1).

2. Experimental section

2.1. Materials

$FeSO_4{\cdot}7H_2O$ was purchased from Basf Chemical Co., Ltd. (Tianjin, China). $NaNO_3$, $C_6H_5Na_3O_7{\cdot}2H_2O$ (citric acid), NaOH, dichloromethane (CH_2Cl_2), 30% H_2O_2, glucose, lactose, fructose, sucrose and maltose were obtained from Guangcheng Reagent Co. (Tianjin, China). 3,3′,5,5′-tetramethylbenzidine dihydrochloride (TMB·2HCl) were purchased from Solarbio Co. (Beijing, China). Glucose oxidase (GOx, 10 KU) was obtained from Sigma-Aldrich and stored at -20 °C in a refrigerator. All chemicals were of analytical grade and used as received without further purification. 5,10,15-tri(4-chlorophenyl)corrole (Corrole), shown in Fig. 1, was prepared according to the previous literature.[35]

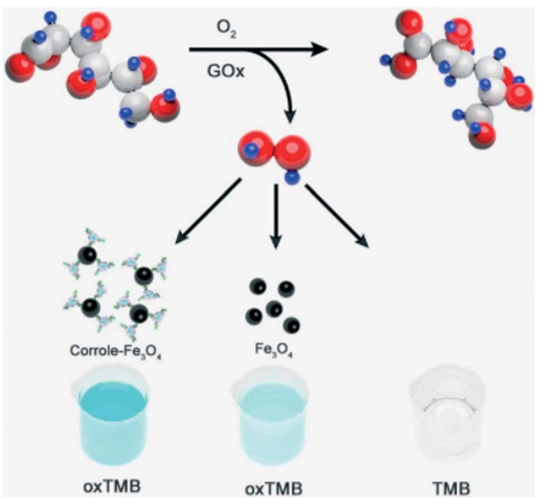

Scheme 1 Schematic illustration of a colorimetric sensor for glucose detection using glucose oxidase (GOx) and Corrole-Fe_3O_4 catalyzed reactions.

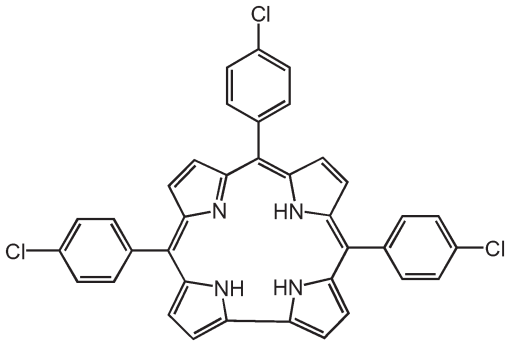

Fig. 1 The molecular structure of 5,10,15-tri(4-chlorophenyl)corrole.

2.2. Preparation of the Corrole-Fe_3O_4 nanocomposites

The Corrole-Fe_3O_4 nanocomposites were synthesized by a facile two-step method. First, the Fe_3O_4 MNPs were prepared according to a reported procedure with a slight modification.[48] Typically, a solution containing 4 mmol of NaOH, 1 mmol of $C_6H_5Na_3O_7{\cdot}2H_2O$ (citric acid, trisodium salt dehydrate), 0.2 mol of $NaNO_3$ and 19 mL of deionized water was heated to 100 °C. After forming a pellucid solution, 1 mL of $FeSO_4{\cdot}7H_2O$ (2 M) solution was rapidly added into the above mixture (equivalent to 0.10 M Fe^{2+} in the alkali solution), and then the mixed solution was transferred to a Teflon-lined stainless steel autoclave and maintained at 100 °C for 1 h. After cooling down to room temperature naturally, the Fe_3O_4 NPs were separated from the resulting solution using a magnet, washed with deionized water for several times and dried at 50 °C for 8 h.

Corrole-Fe_3O_4 nanocomposites were prepared as follows: firstly, Corrole (1 mg) was dissolved into CH_2Cl_2 solution (1 mL). Secondly, the as-prepared Fe_3O_4 nanoparticles (30 mg) dispersed into CH_2Cl_2 solution (10 mL) were then added into the above solution. Finally, the mixed solution was stirred vigorously for 3 h. After that, the product was separated by a magnet, washed with CH_2Cl_2 and absolute ethanol for several times and dried at room temperature.

2.3. Characterization

The crystal structures of the products were measured on a powder X-ray diffractometer (XRD) with a graphite monochromatized Cu Kα radiation (D/Max 2500 PC, Rigaku). The operation voltage and current were kept at 40 kV and 40 mA. The morphology of the nanoparticles was obtained by scanning electron microscopy (SEM, JEOL, Japan). Energy dispersive X-ray spectroscopy (EDS) was carried out to identify the elemental composition of the products. The fluorescent spectra were obtained using an F-4600 FLSPECTOROPHOTOMET spectrofluorophotometer (Hitachi High-Tech Science Corporation, Tokyo, Japan). UV-vis absorption spectra were recorded on a MAPADA UV-3200PC spectrophotometer (Shanghai, China).

2.4. Peroxidase-like catalytic activity

Different colorimetric reaction systems included: (a) 1.0 mM TMB, 0.25 M H_2O_2, 0.4 mg mL^{-1} Corrole-Fe_3O_4 in 0.2 M acetate buffer (pH 3.8); (b) 1.0 mM TMB, 0.25 M H_2O_2, 0.4 mg mL^{-1} Fe_3O_4 in 0.2 M acetate buffer (pH 3.8); (c) 1.0 mM TMB, 0.25 M H_2O_2, in 0.2 M acetate buffer (pH 3.8); (d) 1.0 mM TMB, 0.4 mg mL^{-1}

© Engineered Science Publisher LLC 2018

Corrole-Fe_3O_4 in 0.2 M acetate buffer (pH 3.8); (e) 1.0 mM TMB in 0.2 M acetate buffer (pH 3.8), respectively.

2.5. Reaction mechanism assay

The kinetic measurements were carried out in a time course by monitoring the absorbance at 652 nm on a UV-vis spectrophotometer. For the kinetic assay of H_2O_2, TMB (1mM) was added in 1.4 mL buffer with various concentrations of H_2O_2. Similarly, H_2O_2 (0.25 M) was added in 1.4 mL buffer with various concentrations of TMB for the kinetic assay of TMB. Unless otherwise stated, experiments were implemented in a buffer solution (0.2 mM, pH 3.8, 2 mL) by using 200 μL of Corrole-Fe_3O_4 as enzyme mimics (4 mg/mL). The kinetic parameters were calculated according to the Lineweaver-Burk plot [49]: $1/v = (K_m/V_{max})(1/[S] + 1/K_m)$, where v is the initial velocity, V_{max} corresponds to the maximal reaction velocity, [S] means the concentration of substrate and K_m represents the Michaelis-Menten constant.

The catalytic mechanism was further explored by the photoluminescence (PL) technique using terephthalic acid as a probe molecule. Terephthalic acid readily reacts with ·OH to produce 2-hydroxyterephthalic acid, a fluorescent product.[50] The fluorescent spectra were obtained as follows: 200 μL H_2O_2 (0.25 M), 200 μL Corrole-Fe_3O_4 nanocomposites with different concentrations and 200 μL terephthalic acid (0.5 mM) were incubated in 1.4 mL buffer (0.2 mM, pH 3.8) for 1h. Then, the mixture was monitored on a spectrofluorophotometer.

3. Results and discussion

3.1. Characterization of Corrole-Fe_3O_4 nanocomposites.

Fig. 2 shows XRD patterns of the Fe_3O_4 MNPs and Corrole-Fe_3O_4 nanocomposites, respectively. The strong and sharp peaks at 2θ = 30.2°, 35.5°, 43.2°, 53.4°, 57.0° and 62.6° can be assigned to the (220), (311), (400), (422), (511) and (440) crystalline planes of Fe_3O_4 MNPs, respectively. In addition, these peaks were in well accordance with the standard PDF card (JCPDS card No.75-1610) of Fe_3O_4, indicating that the modification of Corrole did not change the phase of Fe_3O_4 NPs.

Fig. 3 shows the morphologies of Fe_3O_4 MNPs and Corrole-Fe_3O_4 nanocomposites imaged by SEM, respectively. It can be seen from Fig. 3A that the pure Fe_3O_4 MNPs are composed of sphere-like nanoparticles. Meanwhile, slight aggregations were also observed shown in Fig. 3A, due to their magnetic properties. Fig. 3B indicates that Corrole-Fe_3O_4 nanocomposites almost inherited the morphologies of pure Fe_3O_4 MNPs.

The composition of the Corrole-Fe_3O_4 MNPs was further confirmed by means of energy dispersive X-ray analysis (Fig. 4). As shown in Fig. 4, it can be found that the characteristic peaks of C, N, Cl, O and Fe elements deriving from Corrole and Fe_3O_4, respectively, could be detected, indicating the successful preparation of Corrole-Fe_3O_4 MNPs.

The magnetic behavior of the obtained Corrole-Fe_3O_4 nanocomposite was characterized by using a magnet. As shown in Fig. 5, well-dispersed Corrole-Fe_3O_4 nanocomposites could be collected within 3 min when the magnet was put near as-prepared samples. On one hand, the result indicates the Corrole-Fe_3O_4 nanocomposites exhibit excellent magnetic property. On the other hand, benefiting from the magnetic properties, a simple and rapid magnetic separation approach was achieved, showing the possibility of easy recycling for extensive applications such as catalysis.

3.2. Peroxidase-like catalytic activity of the Corrole-Fe_3O_4 nanocomposites

The peroxidase-like activity of the as-prepared Corrole-Fe_3O_4 composites was evaluated through the catalysis between a colorless peroxidase substrate, 3,3′,5,5′-tetramethylbenzidine (TMB), and H_2O_2 to generate a colorimetric reaction. Fig. 6 presents the time-dependent absorbance changes of different reaction systems at 652 nm. Obviously, it can be found that there is a remarkable increase in absorbance of Corrole-Fe_3O_4-H_2O_2-TMB system, but very weak increases of Fe_3O_4-H_2O_2-TMB system, and almost no change for the other three systems: H_2O_2-TMB, Corrole-Fe_3O_4-TMB and TMB system, respectively. Furthermore, the corresponding color differences further reveal the enhanced peroxidase-like activity of the Corrole-Fe_3O_4 composites. These results suggested that in the presence of H_2O_2, the system containing Corrole-Fe_3O_4 nanocomposites produced a deeper color change than that of pure Fe_3O_4 alone, indicating that Corrole-Fe_3O_4 nanocomposites have a higher catalytic activity than that of

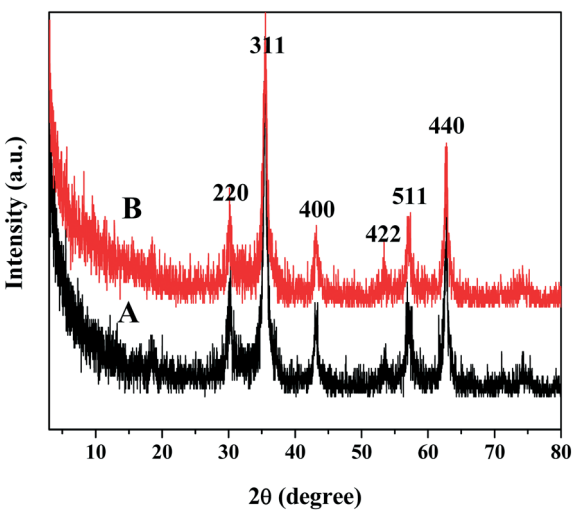

Fig. 2 XRD patterns Fe_3O_4 MNPs (A) and Corrole-Fe_3O_4 MNPs (B), respectively.

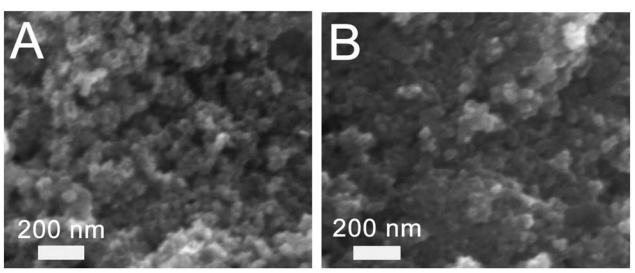

Fig. 3 SEM images of (A) Fe_3O_4 NPs and (B) Corrole- Fe_3O_4 nanocomposites, respectively.

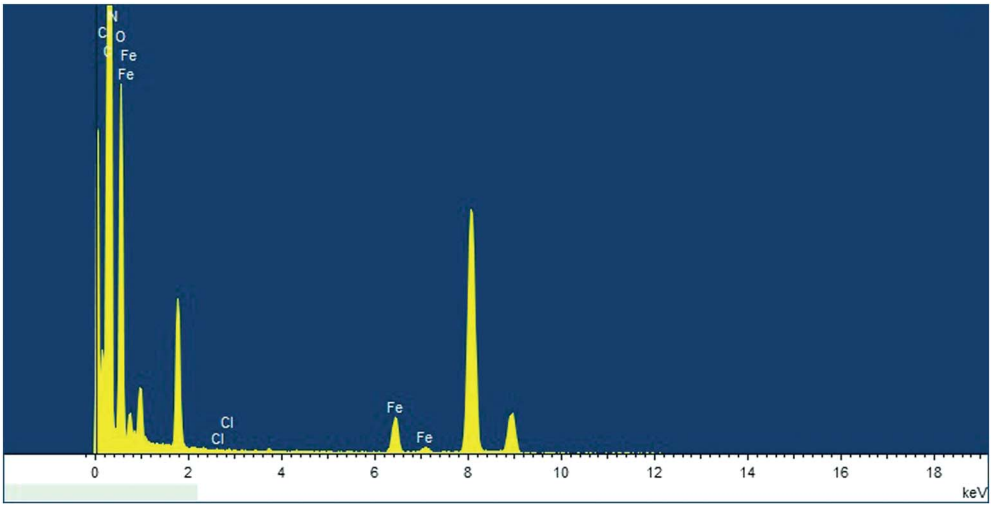

Fig. 4 EDX spectra of Corrole-Fe_3O_4 MNPs.

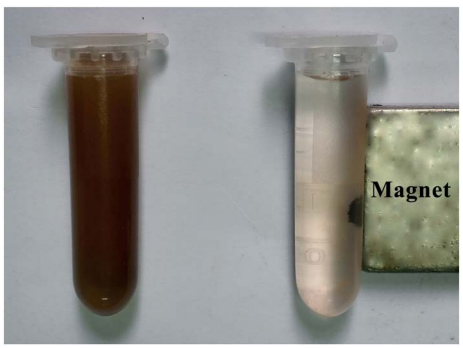

Fig. 5 The photographs of Corrole-Fe_3O_4 suspension in water before and after exposure to a magnet.

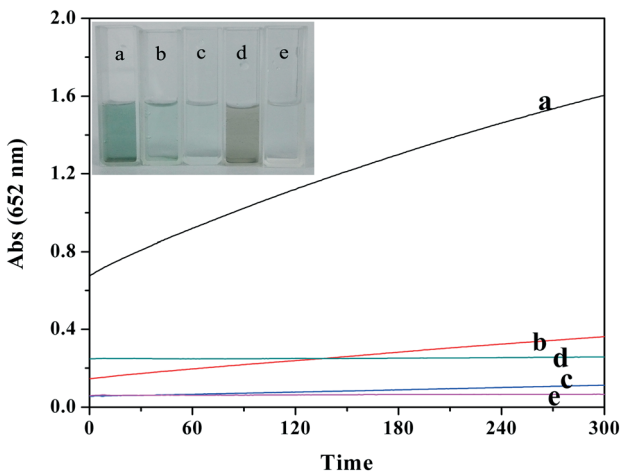

Fig. 6 Time-dependent absorbance evolution at 652 nm of TMB in different reaction systems: (a) TMB + Corrole-Fe_3O_4 + H_2O_2, (b) TMB + Fe_3O_4 + H_2O_2, (c) TMB + H_2O_2, (d) TMB + Corrole-Fe_3O_4, and (e) TMB. The concentrations of TMB, H_2O_2, and Corrole-Fe_3O_4 were 1 mM, 0.25 M, and 0.4 mg mL^{-1}, respectively. The insets represent the corresponding colorimetric photograph.

pure Fe_3O_4 (Fig. 6a and 6b). However, in the absence of Corrole-Fe_3O_4 catalysts or H_2O_2, color change of the different solutions (Fig. 6c, 6d and 6e) is negligible, suggesting that both Corrole-Fe_3O_4 catalysts and H_2O_2 were indispensible for the color reaction. Clearly, these results show that Corrole-Fe_3O_4 demonstrated a much higher catalytic activity than that of pure Fe_3O_4. In addition, to highlight the advantages of our sensing material over the previously reported Fe-based nanostructures as catalysts, we made a comparison of the reaction time required for colorimetric visualization, as listed in Table 1. Obviously, Corrole-Fe_3O_4 exhibits the shortest time response for visual observation.

3.3. Optimization of experimental conditions

As the case of HRP and NPs-based peroxidase mimetics, the catalytic performance of Corrole-Fe_3O_4 is also dependent on pH and temperature (Fig. 7), respectively. The pH-dependent experiments in the range of 1.7-9, shown in Fig. 7A, indicated that the optimal catalytic activity was obtained when pH value was approximately 3.8. The phenomenon was consistent with those of HRP[24] and other nanoenzymes,[24,56] implying that the oxidation of TMB proceeds more easily under weakly acidic conditions than neutral conditions and basic conditions.[55,56] Besides, the effect of temperature on the catalytic activity from 26.5 °C to 66.5 °C was studied. The experimental results showed that the optimal temperature for the Corrole-Fe_3O_4 was 46.5 °C, which was slightly lower than those of IONPs

Table 1 A comparison of the reaction time required for colorimetric visualization using Corrole-Fe_3O_4 nanocomposites and other Fe-based nanostructures as catalysts.

Catalyst	Reaction time	Refs.
CoFe-LDHs	30 min	51
Fe-SBA-15	20 min	52
Fe(III)-polymer nanoparticles	20 min	53
Fe_3O_4 nanoparticles	10 min	10
GO-Fe_3O_4	15 min	54
Corrole-Fe_3O_4	5 min	This work

© Engineered Science Publisher LLC 2018

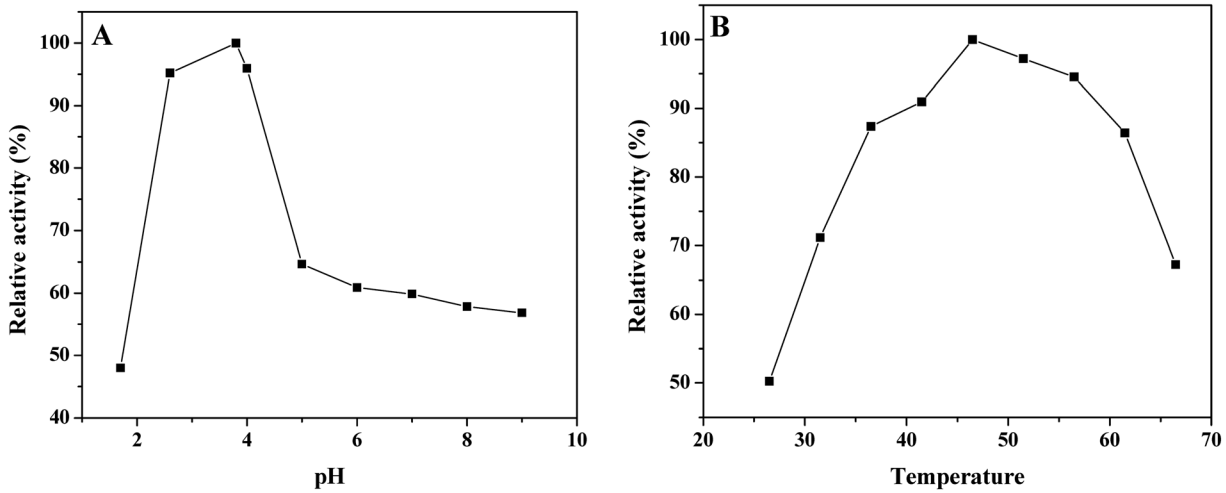

Fig. 7 The influence of buffer pH (A) and incubation temperature (B) on the catalytic activity of the reaction system at 652 nm with the as-synthesized Corrole-Fe_3O_4 nanocomposites as peroxidase mimetics.

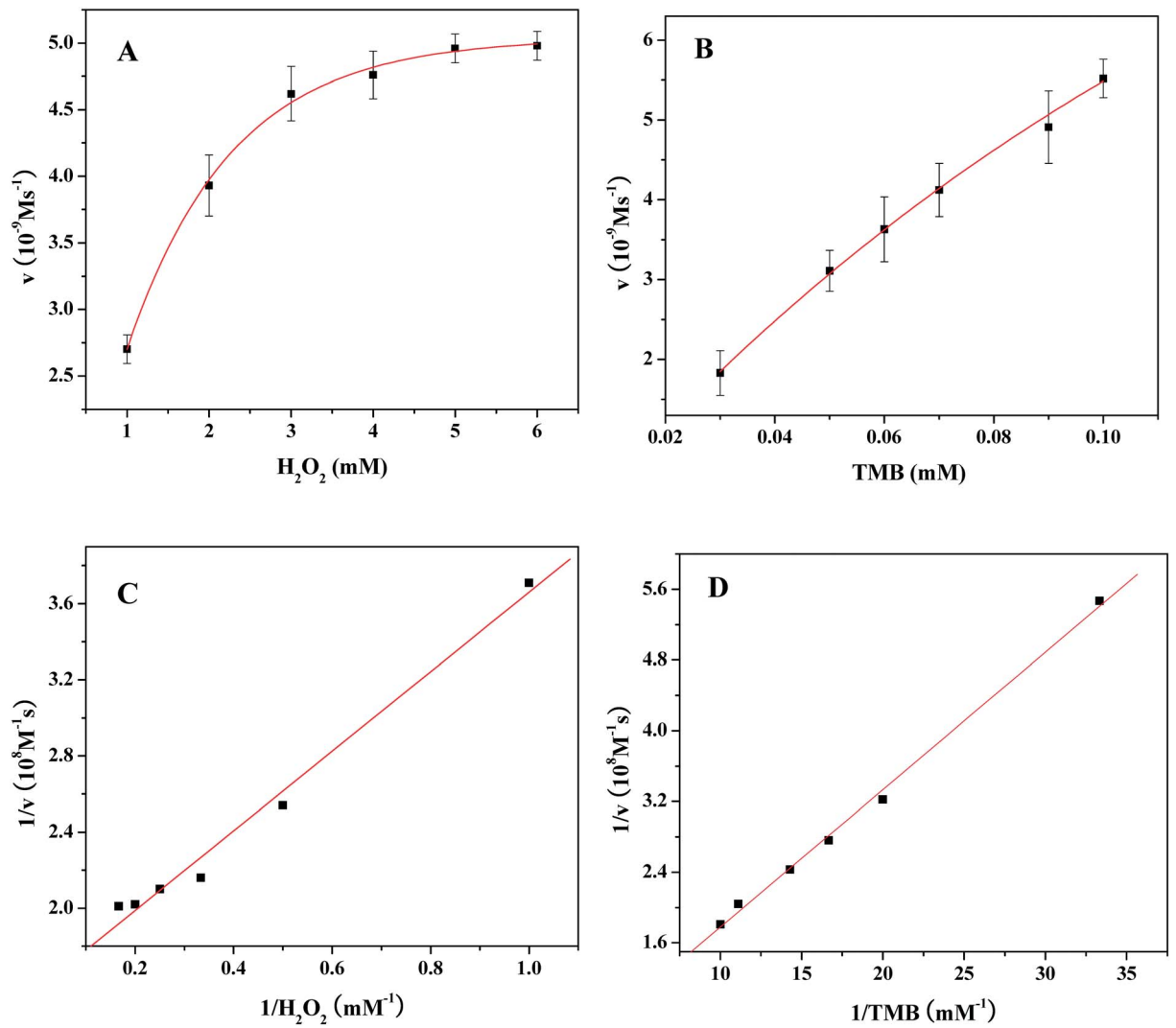

Fig. 8 Steady-state kinetic assay and catalytic mechanism of the Corrole-Fe_3O_4 nanocomposites. (A) The concentration of TMB was 1 mM and the H_2O_2 concentration was varied. (B) The concentration of H_2O_2 was 0.25 M and the TMB concentration was varied. (C and D) Double reciprocal plots of catalytic activity of Corrole-Fe_3O_4 nanocomposites with the concentration of one substrate (H_2O_2 or TMB) fixed and the other varied.

© Engineered Science Publisher LLC 2018

(T = 50 °C)[57] and H@M composite (T=50 °C).[58] Thus, the optimal pH and temperature are approximately pH 3.8 and 46.5 °C, respectively.

3.4. The steady-state kinetic analysis

The peroxidase-like activity of Corrole-Fe_3O_4 enzyme mimics was further explored by performing steady-state kinetic studies. A series of kinetic data with H_2O_2 and TMB as substrates were acquired by changing one substrate concentration while leaving the other concentration constant. It was found that these kinetic data could fit well to typical Michaelis-Menten curves (Fig. 8A and 8B), which was similar in the kinetic behavior to those of nature HRP enzyme[24] and reported peroxidase mimics.[54,59] Michaelis-Menten constant (K_m) and the maximum initial velocity (V_{max}) listed in Table 2 were calculated by using Lineweaver-Burk double-reciprocal plots (Fig. 8C and 8D). As we all know, K_m is generally used to measure the affinity of a given enzyme toward the substrate: the smaller the value of K_m, the stronger the affinity between the enzyme and the substrate. From Table 2, the K_m value of Corrole-Fe_3O_4 with H_2O_2 as substrate was 1.33 mM, which was much lower than HRP[24] and other Fe-based peroxidase mimetics, indicating that Corrole-Fe_3O_4 had a higher affinity for H_2O_2 than that of HRP[24] and other Fe-based peroxidase mimetics.[31,59,60] On the other hand, the K_m value of Corrole-Fe_3O_4 with TMB as a substrate was determined to be 0.697 mM, which was much higher than that of HRP and other Fe-based peroxidase mimetics[31,32,54,60] except for $ZnFe_2O_4$,[59] suggesting that Corrole-Fe_3O_4 had a lower affinity for TMB than that of HRP[24] and other Fe-based peroxidase mimetics,[31,32,54,60] while it had a higher affinity for TMB than that of $ZnFe_2O_4$.[59]

3.5. Mechanism studies on catalytic reaction

The catalytic mechanism of the peroxidase-like of the Corrole-Fe_3O_4 nanocomposites was assumed to result from the decomposition of H_2O_2 into •OH during the reactions, similar to previous peroxidase mimics.[61–63] This hypothesis was confirmed by signal intensity of the fluorescence spectra. As shown in Fig. 9, it can be clearly seen that signal intensity gradually increased with increasing the amount of Corrole-Fe_3O_4 nanocomposites. In other words, the larger amount of Corrole-Fe_3O_4 NPs, the higher yield of •OH. The result shows that Corrole-Fe_3O_4 NPs have excellent intrinsic peroxidase-like activity and accelerate the decomposition of H_2O_2 to generate a high yield of •OH, consistent with previous works such as H_2TCPP-NiO nanorods[64] and H_2TCPP-Fe_3O_4 nanoparticles.[32]

Table 2 Comparison of the apparent Michaelis-Menten constant (K_m) and maximum reaction rate (V_{max}).

catalyst	Substrate	K_m (mM)	V_{max} (10^{-8} M s^{-1})	Ref
Corrole-Fe_3O_4	H_2O_2	1.33	0.6372	This work
Corrole-Fe_3O_4	TMB	0.697	4.482	This work
Fe_3O_4	H_2O_2	154	9.78	14
Fe_3O_4	TMB	0.098	3.44	14
$ZnFe_2O_4$	H_2O_2	1.66	7.74	43
$ZnFe_2O_4$	TMB	0.85	13.31	43
PBMNPs3	H_2O_2	323.6	117	19
PBMNPs3	TMB	0.307	106	19
GO-Fe_3O_4	H_2O_2	0.71	5.31	39
GO-Fe_3O_4	TMB	0.43	13.08	39
Casein-Fe_3O_4	H_2O_2	4.75	15.9	44
Casein-Fe_3O_4	TMB	0.021	10.6	44
H_2TCPP-Fe_3O_4	H_2O_2	0.919	1.075	32
H_2TCPP-Fe_3O_4	TMB	0.439	19.08	32
HRP	H_2O_2	3.70	8.71	14
HRP	TMB	0.434	10	14

3.6. H_2O_2 detection using the Corrole-Fe_3O_4 nanocomposites as peroxidase mimetics

In light of the catalytic activity of Corrole-Fe_3O_4 depends on the concentration of H_2O_2, the system discussed above could be applied to detect H_2O_2. Under optimal conditions, the H_2O_2 concentration-response curve was plotted in Fig. 10A, showing that the response signal gradually increases with increasing H_2O_2 concentration. Fig. 10B manifests the calibration curve of absorbance at 652 nm versus H_2O_2 concentration. A linear range from 10 μM to 100 μM was observed with the limit of detection as low as 3.6 μM. It is found that the detection limit of Corrole-Fe_3O_4 nanocomposites is of the same order of magnitude as that of Fe_3O_4 nanoparticles (3 μM)[10] and Cu-SBA-15 sample (3.7 μM),[65] lower than that of [FeIII(biuret-amide)] on mesoporous silica (10 μM).[66]

3.7. Glucose detection using the Corrole-Fe_3O_4 nanocomposites as peroxidase mimetics

H_2O_2 is an important by-product involved in many biochemical reactions, such as the glucose oxidase (GOx)-catalyzed oxidation reaction of glucose. Additionally, Glucose detection related to human health levels is of vital importance in common analysis. Based on results of the study, a colorimetric quantitative test of glucose can be realized using the Corrole-Fe_3O_4 nanocomposites combined with GOx. Fig. 11A shows a typical glucose concentration-response curve. It can be found that absorbance signal increases gradually with increasing glucose concentration. The corresponding calibration

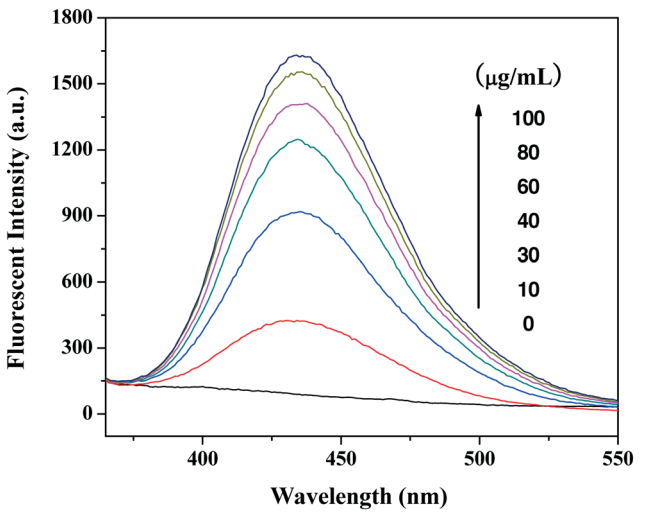

Fig. 9 Fluorescence spectra of terephthalic acid (TA) in the presence of H_2O_2 and Corrole-Fe_3O_4 with different concentrations. The reaction was performed in 1.4 mL NaAc buffer (0.2 mM, pH 3.8) containing 0.5 mM TA, 0.25 M H_2O_2 and Corrole-Fe_3O_4 with different concentrations, the total volume is 2 mL. The excitation wavelength (EX) is at 315 nm.

© Engineered Science Publisher LLC 2018

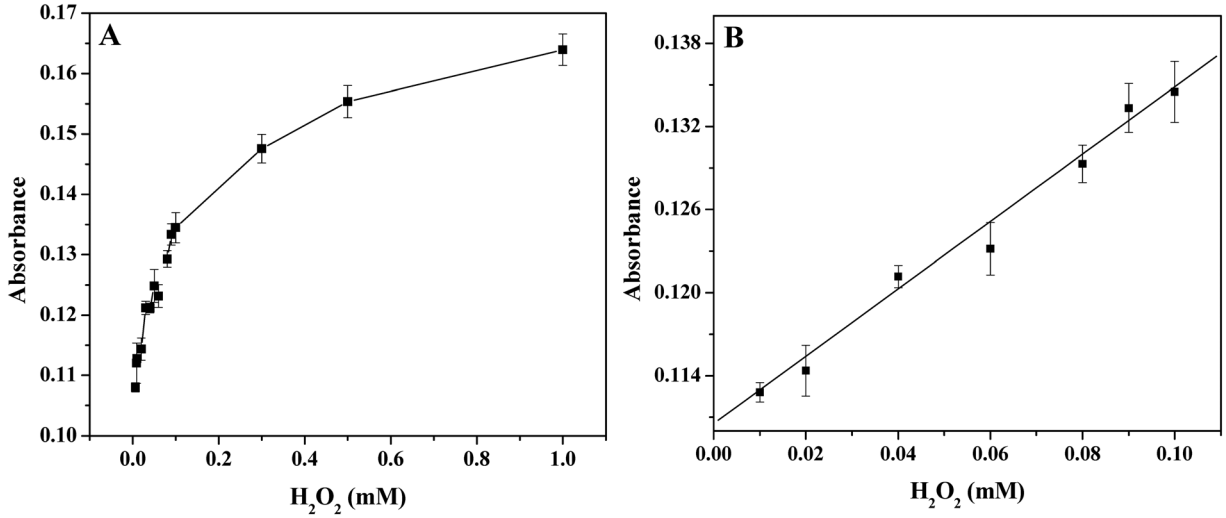

Fig. 10 (A) A dose-response curve for H_2O_2 using Corrole-Fe_3O_4 nanocomposites. (B) The linear calibration plot for the detection of H_2O_2 at 652 nm. Error bars represent the standard deviation based on three repeated measurements.

plot was described in Fig. 11B. The absorbance was linearly related to glucose concentration range from 4 μM to 40 μM. The limit of detection was 25 calculated to be 2.46 μM (S/N=3). The results show that our sensing method presents a reasonable linear response range compared to some reported nanomaterials.[32,54,59,60,67] More significantly, the limit of detection is lower than Fe-based peroxidase mimetics like Fe_3O_4 magnetic nanoparticles (30 μM),[10] GCNT-Fe_3O_4 nanocomposite (22 μM),[68] [FeIII(biuret-amide)] on mesoporous silica (10 μM)[50] and MnSe-g-C_3N_4 peroxidase mimetics (8 μM),[69] indicating a more sensitivity of Corrole-Fe_3O_4 MNPs.

To examine the selectivity of the present method toward glucose, detection experiments using maltose, sucrose, lactose and fructose as control samples were investigated (Fig. 12). It can be obviously found that the absorbance of these glucose analogues was not obvious even when their concentrations were 5 times as high as glucose. The color difference also can be detected visually from the corresponding photographs (Fig. 12 inset). These results demonstrated that the method developed here has high selectivity toward glucose detection

4. Conclusions

In conclusion, the Corrole-Fe_3O_4 nanocomposites were prepared for the first time by a facile two-step approach and developed as an enhanced peroxidase mimetic. Furthermore, the introduction of Corrole could significantly improve peroxidase-like activity of the Fe_3O_4, which could be observed visually from both the absorbance data and photographs before and after modification by Corrole. More importantly, the optimization results indicate the catalytic activity of the Corrole-Fe_3O_4 is sensitive to variations of pH and temperature. The affinity features for H_2O_2 and TMB were applicable to quantitative determination of H_2O_2 and glucose, exhibiting reasonable response

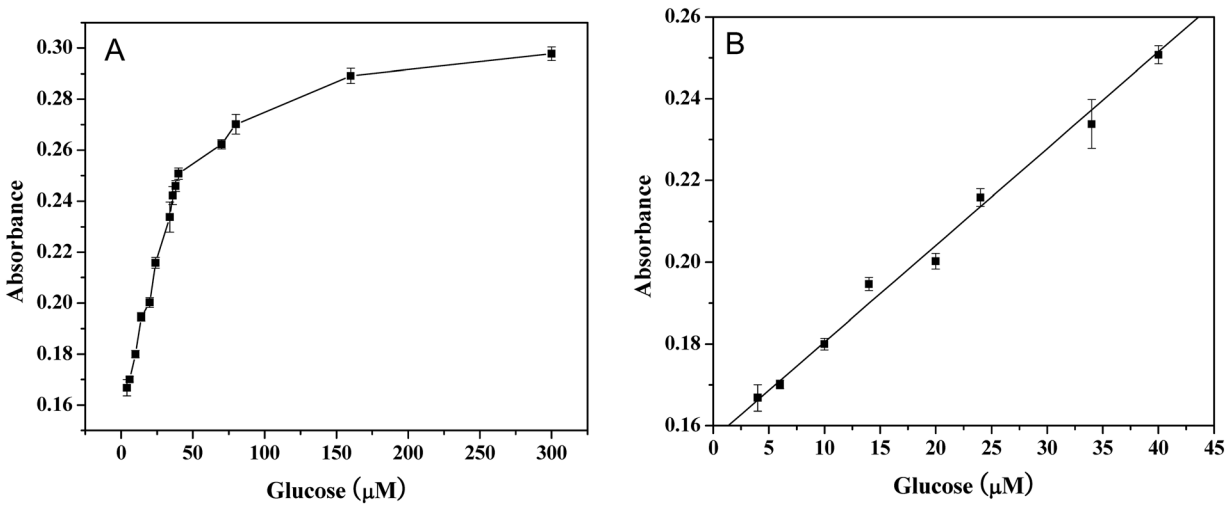

Fig. 11 (A) A dose-response curve for glucose detection using Corrole-Fe_3O_4 nanocomposites. (B) The linear calibration plot for glucose. Error bars represent the standard deviation based on three repeated measurements.

© Engineered Science Publisher LLC 2018

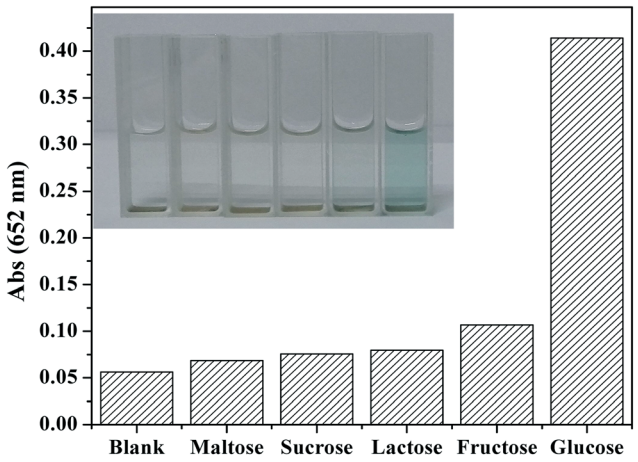

Fig. 12 Determination of the selectivity of glucose detection (from left to right: blank, 5 mM maltose, 5 mM sucrose, 5 mM lactose, 5 mM fructose and 1 mM glucose). Inset: the color difference with different samples.

range and low limit of detection, respectively. Given the advantages of low cost, easy separation, facial fabrication, fast response and good selectivity, it can be expected that the novel Corrole-Fe_3O_4 nanocomposites as a peroxidase mimetic may broaden the scope of its applications in the field of catalysis and bioassays.

Acknowledgments

Financial support from the National Natural Science Foundation of China (Grant no. 21271119), Natural Science Foundation of Shandong Province (Grant No. ZR2018MB002, ZR2018MEE003) and Scientific Research Foundation of Shandong University of Science & Technology (Grant No.2015RCJJ018).

References

1 K.S. Park, M.I. Kim, D.Y. Cho and H.G. Park, *Small*, 2011, **7**, 1521–1525.
2 I.B. Burgess, M. Loncar and J. Aizenberg, *J. Mater. Chem. C*, 2013, **1**, 6075–6086.
3 K.Y. Pu and B. Liu, *Adv. Funct. Mater.*, 2009, **19**, 1371–1378.
4 Q. Liu, P. Chen, Z. Xu, M. Chen, Y. Ding, K. Yue and J. Xu, *Sensor Actuat. B: Chem.*, 2017, **251**, 339–348.
5 L. Zhang, M. Chen, Y. Jiang, M. Chen, Y. Ding and Q. Liu, *Sensor Actuat. B: Chem.*, 2017, **239**, 28–35.
6 L. Sun, Y. Ding, Y. Jiang and Q. Liu, *Sensor Actuat. B: Chem.*, 2017, **239**, 848–856.
7 M. Chen, Y. Ding, Y. Gao, X. Zhu, P. Wang, Z. Shi and Q. Liu, *RSC Adv.*, 2017, **7**, 25220–25228.
8 Q. Liu, Y. Ding, Y. Yang, L. Zhang, L. Sun, P. Chen and C. Gao, *Mater. Sci. Eng. C*, 2016, **59**, 445–453.
9 Q. Liu, Y. Jiang, L. Zhang, X. Zhou, X. Lv, Y. Ding, L. Sun, P. Chen and H. Yin, *Mater. Sci. Eng. C*, 2016, **65**, 109–115.
10 H. Wei and E.K. Wang, *Anal. Chem.*, 2008, **80**, 2250–2254.
11 Y. Ding, L. Sun, Y. Jiang, S. Liu, M. Chen, M. Chen, Y. Ding and Q. Liu, *Mater. Sci. Eng. C*, 2016, **67**, 188–194.
12 Q. Liu, Y. Yang, X. Lv, Y. Ding, Y. Zhang, J. Jing and C. Xu, *Sensor Actuat. B: Chem.*, 2017, **240**, 726–734.
13 L. Zhang, Y. Li, Q. Zahng and H. Wang, *CrystEngComm*, 2013, **15**, 5986–5993.
14 H. Zhou, Q. Liu, W. Liu, J. Ge, M. Lan, C. Wang, J. Geng and P. Wang, *Chem. Asian J.*, 2014, **9**, 811–818.
15 J.B. Zhang, J. Zhuang, L.Z. Gao, Y. Zhang, N. Gu, J. Feng, D.L. Yang, J.D. Zhu and X.Y. Yan, *Chemosphere*, 2008, **73**, 1524–1528.
16 W. Luo, L.H. Zhu, N. Wang, H.Q. Tang, M.J. Cao and Y.B. She, *Environ. Sci. Technol.*, 2010, **44**, 1786–1791.
17 X.B. Hu, B.Z. Liu, Y.H. Deng, H.Z. Chen, S. Luo, C. Sun, P. Yang and S.G. Yang, *Appl. Catal. B: Environ.*, 2011, **107**, 274–283.
18 J. Kim, H.S. Kim, N. Lee, T. Kim, H. Kim, T. Yu, I.C. Song, W. K. Moon and T Hyeon, *Angew. Chem., Int. Ed.*, 2008, **47**, 8438–8441.
19 Y. Pan, X. Du, F. Zhao and B. Xu, *Chem. Soc. Rev.*, 2012, **41**, 2912–2942.
20 M.A. Gijs, F.D.R. Lacharme and U. Lehmann, *Chem. Rev.*, 2010, **110**, 1518–1563.
21 C. Bergemann, D. Muller-Schulte, J. Oster, L.A. Brassard and A.S. Lubbe, *J. Magn. Magn. Mater.*, 1999, **194**, 45–52.
22 A. Ito, E. Hibino, C. Kobayashi, H. Terasaki, H. Kagami, M. Ueda, T. Kobayashi and H. Honda, *Tissue Eng.*, 2005, **11**, 489–496.
23 H.H. Yang, S.Q. Zhang, X.L. Chen, Z.X. Zhuang, J.G. Xu and X. R. Wang, *Anal. Chem.*, 2004, **76**, 1316–1321.
24 L. Gao, J. Zhuang, L. Nie, J. Zhang, Y. Zhang, N. Gu, T. Wang and X.Y. Yan, *Nat. Nanotechnol.*, 2007, **9**, 577–583.
25 N. Ding, N. Yan, C. Ren and X.G. Chen, *Anal. Chem.*, 2010, **82**, 5897–5899.
26 M.M. Liang, K.L. Fan, Y. Pan, H. Jiang, F. Wang, D.L. Yang, D. Lu, J. Feng, J.J. Zhao, L. Yang and X.Y. Yan, *Anal. Chem.*, 2013, **85**, 308–312.
27 Y. Ding, B. Yang, H. Liu, Z. Liu, X. Zhang, X. Zheng and Q. Liu, *Sensor Actuat. B: Chem.*, 2018, **259**, 775–783.
28 Y. Ding, M. Chen, K. Wu, M. Chen, L. Sun, Z. Liu, Z. Shi and Q. Liu, *Mater. Sci. Eng. C*, 2017, **80**, 558–565.
29 J.Z. Chen, Y.J. Liu, G.X. Zhu and A.H. Yuan, *Cryst. Res. Technol.*, 2014, **49**, 309–314.
30 J.W. Lee, H.J. Jeon, H.J. Shin and J.K. Kang, *Chem. Commun.*, 2012, **48**, 422–424.
31 X.Q. Zhang, S.W.Y. Gong, Y. Zhang, T. Yang, C.Y. Wang and N. Gu, *J. Mater. Chem.*, 2010, **20**, 5110–5116.
32 Q. Liu, H. Li, Q Zhao, R. Zhu, Y. Yang, Q Jia, B. Bian and L. Zhuo, *Mater. Sci. Eng. C*, 2014, **41**, 142–151.
33 Q. Liu, L. Zhang, H. Li, Q.Y Jia, Y. Jiang, Y. Yang and R. Zhu, *Mater. Sci. Eng. C*, 2015, **55**, 193–200.
34 M. Chen, L. Sun, Y. Ding, Z. Shi and Q. liu, *New J. Chem.*, 2017, **41**, 5853–5862.
35 G.F. Lu, S. Yan, M.Y. Shi, W.H. Yu, J. Li, W.H. Zhu, Z.P. Oua and K.M. Kadish, *Chem. Commun.*, 2015, **51**, 2411–2413.
36 K.M. Kadish, K.M. Smith, R. Guilard, Eds.; Academic Press: San Diego, 2000; Vol. 2, pp 201-232.
37 Z. Gross and H.B. Gray, *Comm. Inorg. Chem.*, 2006, **27**, 61–72.
38 K.M. Kadish, K.M. Smith, R. Guilard, Eds.; Academic Press: San Diego, 2000; Vol. 2, pp 233-300.

 © Engineered Science Publisher LLC 2018

39 I. Aviv-Harel and Z. Gross, *Chem. Commun.*, 2007, **20**, 1987–1999.
40 I. Aviv-Harel and Z. Gross, Aura of Corroles, *Chem. Eur. J.*, 2009, **15**, 8382–8394.
41 K.M. Kadish, K.M. Smith, R. Guilard, Eds.; Academic Press: San Diego, 2003; Vol. 18, pp 303-349.
42 K.M. Kadish, K.M. Smith, R. Guilard, Eds.; Academic Press: Singapore, 2000; Vol. 2, pp 201-232.
43 L. Flamigni and D. T. Gryko, *Chem. Soc. Rev.*, 2009, **38**, 1635–1646.
44 I. Aviv-Harel and Z. Gross, *Coord. Chem. Rev.*, 2011, **255**, 717–736.
45 H. Liu, M.H.R. Mahmood, S. Qiu and C.K. Chang, *Coord. Chem. Rev.*, 2013, **257**, 1306–1333.
46 L.S.H.P Vale, J.F.B. Barata, M.A.F. Faustino, M.G.P.M.S. Neves, A.C. Tomé, A.M.S. Silva and J.A.S. Cavaleiro, *Tetrahedron Lett.*, 2007, **48**, 8904–8908.
47 L.S.H.P. Vale, J.F.B. Barata, C.I.M. Santos, M.G.P.M.S. Neves, M.A.F. Faustino, A.C. Tomé, A.M.S. Silva, F.A.A. Paz and J.A.S. Cavaleiro, *J. Porphyr. Phthalocya.*, 2009, **13**, 358–368.
48 C. Hui, C. Shen, T. Yang, L. Bao, J. Tian, H. Ding, C. Li and H.J. Gao, *J. Phys. Chem. C*, 2008, **112**, 11336–11339.
49 H. Lineweaver and D. Burk, *J. Am. Chem. Soc.*, 1934, **56**, 658–61L.
50 L. L. Ju, Z. Y. Chen, L. Fang, W. Dong, F. G. Zheng and M. R. Shen, *J. Am. Ceram. Soc.*, 2011, **94**, 3418–3424.
51 Y. W. Zhang, J. Tian, S. Liu, L. Wang, X. Qin and X. Sun, *Analyst*, 2012, **137**, 1325–1328.
52 S. Liu, J. Tian and X. Sun, *Analyst*, 2011, **136**, 4894–4897.
53 J. Tian, S. Liu, Y. Luo and X. Sun, *Catal. Sci. Technol.*, 2012, **2**, 432–436.
54 Y.L. Dong, H.G. Zhang, Z.U. Rahman, L. Su, X.J. Chen, J. Hu and X.G. Chen, *Nanoscale*, 2012, **4**, 3969–3976.
55 J. Wang, D. Han, X. Wang, B. Qi and M. Zhao, *Biosens. Bioelectron.*, 2012, **36**, 18–21.
56 S.L. Li, H. Li, F.J. Chen, J. Liu, H.L. Zhang, Z.Y. Yang and B.D. Wang, *Dyes and Pigments*, 2016, **125**, 64–71.
57 A. Mishra1, R. Ahmad1, M. Perwez1 and M. Sardar, *BioNanoSci.*, 2016, 1–10.
58 F.X. Qin, S.Y. Jia, F.F. Wang, S.H. Wu, J. Song and Y. Liu, *Catal. Sci. Technol.*, 2013, **3**, 2761–2768.
59 L. Su, J. Feng, X.M. Zhou, C.L. Ren, H. Li and X.G. Chen, *Anal. Chem.*, 2012, **84**, 5753–5758.
60 Y. Liu, M. Yuan, L.J. Qiao and R. Guo, *Biosen. Bioelectron.*, 2014, **52**, 391–396.
61 Y.L. Guo, X.Y. Liu, C.D. Yang, X.D. Wang, D. Wang, A. Iqbal, W.S. Liu and W. Qin, *ChemCatChem*, 2015, **7**, 2467–2474.
62 X.J. Zheng, Q. Zhu, H.Q. Song, X.R. Zhao, T. Yi, H.L. Chen and X.G. Chen, *ACS Appl. Mater. Interfaces*, 2015, **7**, 3480–3491.
63 X.R. Guo, Y. Wang, F.Y. Wu, Y.N. Ni and S. Kokot, *Analyst*, 2015, **140**, 1119–1126.
64 Q.Y. Liu, Y.T. Yang, H. Li, R. Zhu, Q. Shao, S.G. Yang and J. Xu, *Biosen. Bioelectron.*, 2015, **64**, 147–153.
65 J.S. Mu, Y. He and Y. Wang, *Talanta*, 2016, **148**, 22–28.
66 B. Malvi, C. Panda, B.B. Dhar and S.S. Gupta, *Chem. Commun.*, 2012, **48**, 5289–5291.
67 Q. Li, G. Tang, X. Xiong, Y. Cao, L. Chen, F. Xu and H. Tan, *Sens. Actuator B: Chem.*, 2015, **215**, 86–92.
68 H. Wang, S. Li, Y. Si, Z. Sun, S. Li and Y. Lin, *J. Mater.Chem. B*, 2014, **2**, 4442–4448.
69 F.M. Qiao, Q.Q. Qi, Z.Z. Wang, K. Xu and S.Y. Ai, *Sens. Actuator B: Chem.*, 2016, **229**, 379–386.

© Engineered Science Publisher LLC 2018